Small Signal Study of Grid-forming Converters and Impact of Different Control Structures and Parameters

Luke Benedetti, Panagiotis N. Papadopoulos, Agustí Egea-Álvarez
Department of Electronic and Electrical Engineering
University of Strathclyde – Glasgow, Scotland

***Abstract*—Towards transitioning to a carbon-free power system, new dynamic phenomena and interactions involving grid-forming converters (GFMs) will become important as their proliferation occurs to support this transition. The multi-loop control incorporating inner cascaded voltage and current controllers (VC and CC) often utilised within GFMs are generally expected to cause interactions in higher frequency ranges than the (well-studied) dynamics of interest associated with a purely synchronous machine-based system. However, the restricted control bandwidth associated with low switching frequency of large power rated VSCs results in the need for much slower control time constants, causing potentially destabilizing, lower-frequency (or even non-oscillatory) interactions. This paper offers an extensive insight into the small-signal, multi-machine interactions involving large power rated GFMs in a transmission network: the IEEE 39-bus New-England test system (NETS). Furthering the contribution of this paper, multi-loop controllers are employed within the GFMs, offering an insight into their interactions with other power system elements to help aid the ongoing discussions on model appropriateness and direct AC voltage control versus multi-loop control. Finally, parametric sweep sensitivity analyses are performed for the GFMs which are implemented as virtual synchronous machines (VSMs).**

***Index Terms*—Grid-forming converters, small signal, stability, power system, dynamics.**

I. Introduction

Grid-forming converters (GFMs) are one of the promising solutions for enabling ever increasing penetrations of converter-interfaced generation (CIG), primarily in the form of wind and solar energy resources. In the transitionary period before synchronous generators (SGs) are fully phased out, a combination of SGs, GFMs and grid-following converters (GFLs) are expected to be present in power systems. The interactions among such devices with each other and existing power system elements are of significant interest [1], especially in terms of small-signal behaviour. As of yet, the GFM concept, despite being utilised for microgrid applications [2][3] , has not been fully explored from a small-signal perspective, especially in the context of large, interconnected power systems.

The literature pertaining to GFMs in larger power systems in previous years has been restricted to defining general penetration level limits [4]. More recently, the impact of GFMs on power system stability has been an increasing topic of interest. [5] produced an extensive small signal analysis of CIG from a small, two-machine with infinite bus system, up to a large-scale system in the form of the 59-bus South-East Australian network. This work offers invaluable insights into the nature of the most influential interactions between SGs, GFMs and GFLs, albeit with limited discussion into the nature of the specific modes when in the large system due to a focus on CIG penetration limits. There remains scope to describe extensively the small signal interactions seen in a large-scale power system with GFMs, especially since the most influential interactions can easily change depending on a multitude of factors including operating points as [5] highlights. In terms of GFMs in single machine infinite bus (SMIB) systems, [6][7] and [8] investigate the small signal behaviour of different GFM control schemes with the last of which focusing on tuning through eigenvalue analysis before validation with a modified IEEE 39-bus New-England test system (NETS).

A large proportion of research into GFMs has been focused on the important issue of current limitation [9][10]. Two promising approaches are direct AC voltage control with threshold-induced virtual impedance (TIVI) [9][11] and the use of multi-loop control [12]. The latter constitutes inner cascaded voltage and current controllers (VC and CC), allowing for a limitation to be applied to the current reference generated by the former and applied to the latter. The idea of direct AC voltage control refers to the creation of a voltage phasor from the GFM control section and bypassing inner controllers by applying the reference directly to the AC voltage modulation of the converter terminals. This approach can also incorporate virtual impedance [5] or alternative control such as LQR regulators [9].

Traditionally, inner VCs and CCs are much faster than that of the outer active and reactive power (or voltage magnitude) control. This allows sufficient timescale separation from the inner loops to the outer loop and electromechanical (EMc) dynamics that dominate power systems [5]. In GFMs, the tuning of the inner cascaded controllers has been discussed in [12] and [13], both of which find conventional tuning methods insufficient due to low switching frequencies of voltage source converters (VSCs) at large power ratings. This is due to limited bandwidth of the inner controllers resulting in increased potential for instability. Therefore, through different tuning procedures, [12] and [13] find new parameters which suffice. They are of much higher time constants, and from [13] are the values adopted for the small signal analysis described earlier [5]. Although [12] and [13] displayed the nature of the small signal interactions at conventional tuning, they did not show how this changes after re-tuning.

In this paper, the interaction of these slower inner controller dynamics of multiple, distant GFMs, as well as with the EMc and power system stabiliser (PSS) dynamics of SGs is observed. The main contribution of this paper is a

Financial support is acknowledged from an EPSRC Student Excellence Award Studentship (L. Benedetti), and a UKRI Future Leaders Fellowship (P. Papadopoulos) [MR/S034420/1]. All results can be fully reproduced using the methods and data described in this paper and provided references.

This is a peer-reviewed, accepted author manuscript of the following article: Benedetti, L., Papadopoulos, P. N., & Egea-Alvarez, A. (2022). Small signal study of grid-forming converters and impact of different control structures and parameters. In 2022 IEEE PES Innovative Smart Grid Technologies Conference Europe (ISGT-Europe) IEEE. https://doi.org/10.1109/isgt-europe54678.2022.9960644

comprehensive break down of the small signal interactions which have participation from the virtual synchronous machine (VSM) GFMs [14] found at transmission-scale. Specifically, for the modified NETS network being studied. This is completed for the GFMs utilising direct AC voltage control but also when using multi-loop control. Finally, parametric sweep sensitivity analyses of relevant GFM parameters are performed.

II. Modelling and Analysis Methodology

A. Modelling

The small signal models are developed in state-space representation in accordance with [15]. All modelling has been implemented in MATLAB 2020a, utilising a modular, adaptable coding framework which allows for any power system model to be easily developed provided the parameters of each element and the MATPOWER load flow case file [16] are available. An optimal power flow (OPF) will be performed using MATPOWER, enabling the extraction of initial states for use when setting up the modules along with the dynamic parameter information. Additionally, the small-signal model has been validated using time-domain comparison with a nonlinear model of the system in Simulink.

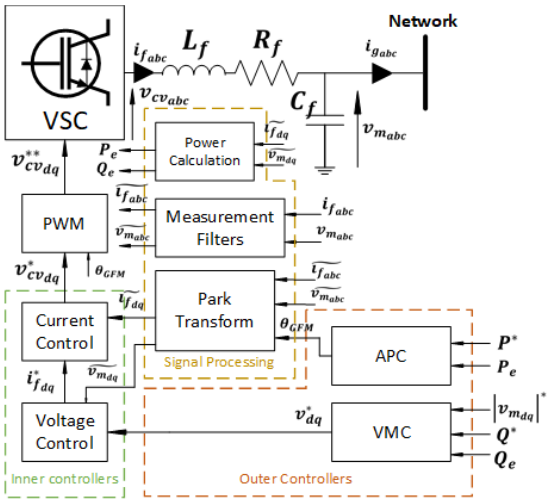

Fig. 1. GFM converter control structure.

SG model: is of the balanced, 8th order machine as in [17]. The SG is also fitted with an AVR/exciter combination of type EXCST1. Additionally, there is a PSS of type PSS1A and finally, there is a governor/turbine combination of type IEEEG1. Implementation of all controllers is found in [18].

GFM model: can be split into four modules and is displayed in Fig. 1. The first is the electrical circuit comprising an output RLC filter. Next is the signal processing whereby the current and voltage measurements are filtered and transformed into the machine's local rotating reference frame (RRF) with signals represented in dq coordinates [19]. This section also includes the calculation of the active and reactive power. Following this, there is the outer loop controls which include the active power controller (APC) implemented as a VSM as in [12]. There is the voltage magnitude controller (VMC), in this case utilising a reactive power-voltage droop as in [12]. Thirdly the inner VC and CC are modelled as in [12]. The output of the inner controls is the voltage modulation signal $v^*_{cv_{dq}}$ which is applied to the fourth and final section, the averaged model converter [19] through a pulse width modulation (PWM) stage approximated by a first-order time delay [12].

Network model: incorporates dynamic PI circuit representations of the transmission lines and dynamic RL circuits for both the transformers and the loads. The network itself is implemented in the RRF of the chosen reference machine meaning the transformation between local and global (system) reference frames require only a geometrical transformation [15]. Additionally, Kirchhoff's current law is applied for the interconnection of all the modules at each bus.

B. IEEE 39-Bus NETS Network

The parameters of the NETS network and the SGs within are adopted from [18]. From the base case presented there, 600 MVA rated GFMs were added at bus locations 5, 16 and 26 as in Fig. 2: each set to output 300 MVA at a power factor of 0.95. Parameters related to GFMs are presented in Table I.

TABLE I. GFM Initial Parameters

Parameter	Value	Parameter	Value
Inertia constant H_{apc}	4 s	R_f	.03 pu
APC damping D_{apc}	10 pu	L_f	.08 pu
Voltage droop m_q	.001 pu	C_f	.074 pu
Inner VC damping factor ζ	25	Measurement filter cut-off f_c	100 Hz
Switching frequency f_s	2 kHz	CC time constant τ_{CC}	$10\times(1/f_s)$
CC $P^\star$ gain K_P^i	.0424 pu	VC $P^\star$ gain K_P^v	.1406 pu
CC $I^\star$ gain K_I^i	6 pu	VC $I^\star$ gain K_I^v	.0108 pu
CC $F^\star$ gain FF_i	0	VC $F^\star$ gain FF_v	1

$I^\star$=integral, $P^\star$=proportional and $F^\star$=feedforward.

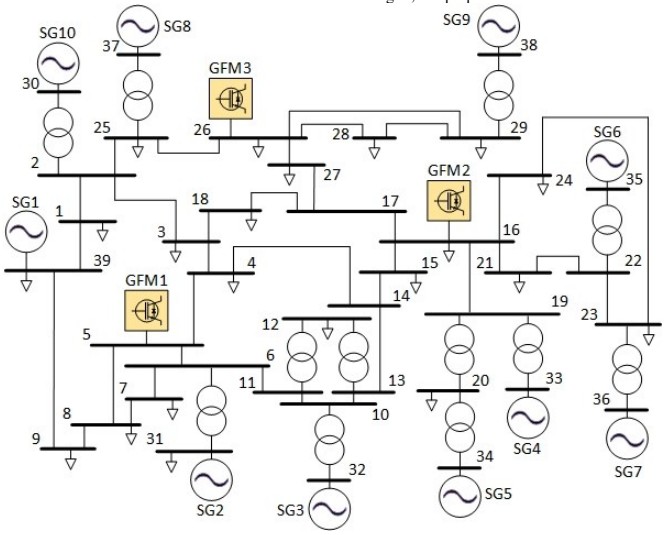

Fig. 2. Modified IEEE 39-bus NETS network.

C. Small Signal Analysis Methodology

Small signal analysis is driven by the calculation of the eigenvalues of the state matrix in a linearised state-space system which relates the state derivatives to the system states [15]. The analysis of these eigenvalues allows us insight into the nature of individual dynamics with information on their frequency, damping, proximity to the unstable region, and participating

states. This last piece of information is extracted through the calculation of participation factors as in [17]:

$$p_{ij} = \left(|\psi_{ij}| \times |\phi_{ij}|\right) \Big/ \left(\sum_{i=1}^{n} |\psi_{ij}| \times |\phi_{ij}|\right) \quad (1)$$

where ψ and ϕ are the left and right eigenvectors. The subscript 'ij' refers to the contribution of the i^{th} state to the j^{th} eigenvalue and the value n refers to the total number of states.

To classify the GFM dominant eigenvalues, a minimum participation from the sum of all GFM states of 10% is required. Additionally, any eigenvalue that was fully damped with real value less than -10 was considered irrelevant. It was found that those eigenvalues with participation from only GFM output filter states and network states were extremely stable and had no sensitivity to any GFM control parameters. Therefore, the output filter states were not considered GFM states when determining the modes of interest. Note, this might not be true with higher bandwidth inner controllers. The determination of relevant eigenvalues was performed for the direct AC voltage control scenario before the inner VCs and CCs are added to the GFMs. The initial tuning for these inner controllers were determined using the modulus optimum technique for the CC and the symmetrical optimum approach for the VC [12]. The latter requires a damping factor to be chosen which is obtained in this case from a parametric sweep displayed in Fig. 3a. All further information regarding the parametric sweeps can be found in the Fig. 3 caption, including a zoom key to clarify which mode category (section IV) is being displayed.

Knowing the eigenvalues that exist is not sufficient as we require an idea of how the important system parameters impact the stability of these eigenvalues to gain a complete picture. Therefore, parametric sweep based sensitivity analyses are performed to determine how the dynamics are impacted. This involves eigenvalue plots for a parameter value being considered across an appropriate range with all other parameters held constant. In this work, the sensitivity analysis is performed only for the multi-loop scenario.

III. GFMs with Direct AC Voltage Control

This section regards the analysis performed on the test system described previously with all GFMs implemented without the inner controllers. That is, they employ direct AC voltage control. All eigenvalues of interest are shown in Table II along with their frequency, damping ratio and most dominant states, characterized by a minimum of 5% participation factor unless stated otherwise. Those with participation above 10% are presented in bold.

There are six modes in the range of 21.63 Hz to 21.66 Hz. These modes have participation purely from the input measurement filters of the GFMs. They are very well damped with damping ratio of approximately 0.869 and do not move throughout parametric sweeps and so have not been included in Table II. Similar modes were found in the multi-loop scenario and again have not been included in Table III or the display of the parametric sweeps in Fig. 3.

All of the eigenvalues are seen to be in the EMc range with frequencies between 1.1862 Hz and 1.9422 Hz. The EMc nature

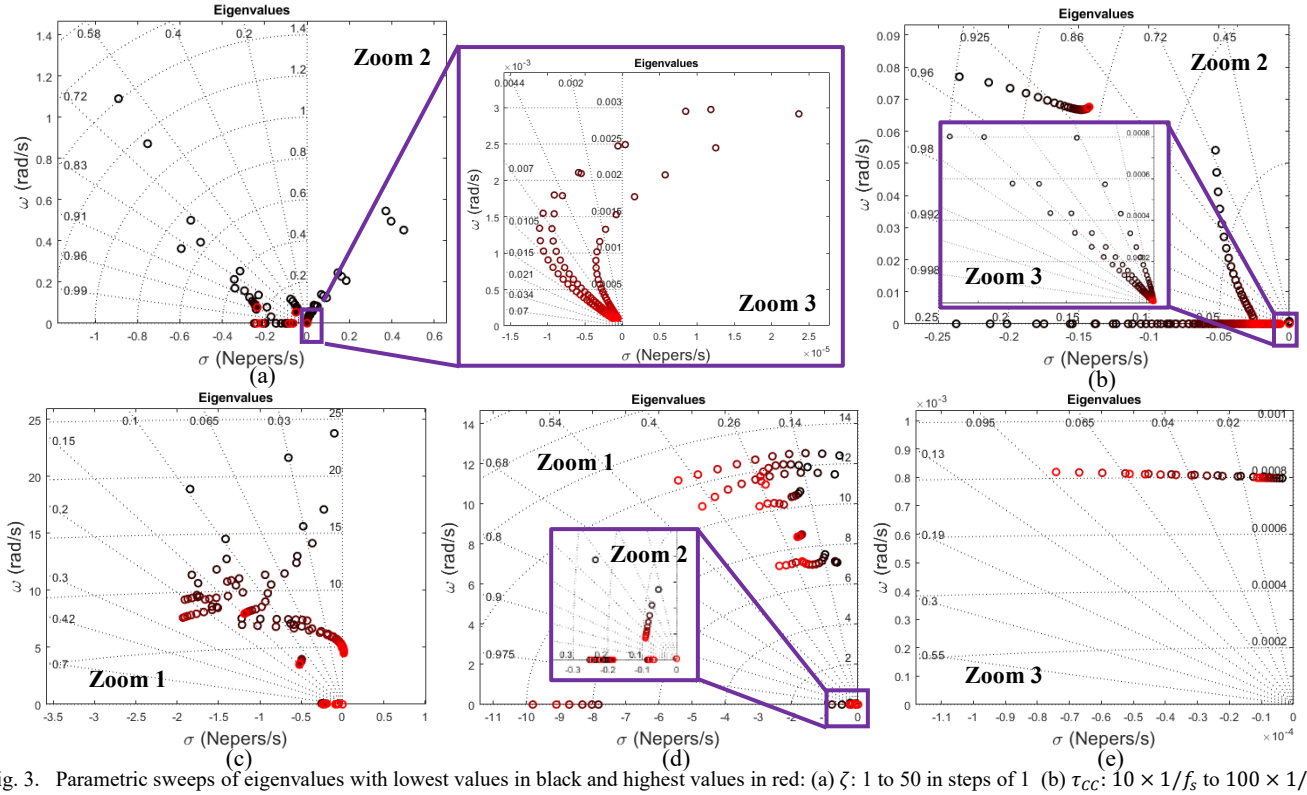

Fig. 3. Parametric sweeps of eigenvalues with lowest values in black and highest values in red: (a) ζ: 1 to 50 in steps of 1 (b) τ_{CC}: $10 \times 1/f_s$ to $100 \times 1/f_s$ in steps of $1.8 \times 1/f_s$, (c) H: 2s to 50s in steps of 2s, (d) D_{apc}: 10 to 100 in steps of 10 and (e) m_q: 0.1 % to 1 % in steps of 0.1 %. Zoom key: 1=electromechanical modes, 2=inner CC-related modes, 3-inner VC-related modes.

TABLE II. EIGENVALUES OF INTEREST FOR DIRECT AC VOLTAGE CONTROL SCENARIO

Eigenvalue	Coordinates	Frequency (Hz)	Damping Ratio	Dominant States	Category
$\lambda_{1\&2}$	$-0.5879 \pm j12.2031$	1.9422	0.0481	$\boldsymbol{\omega_{GFM_2}}$,$\boldsymbol{\delta_{GFM_2}}$,$\omega_{r_4}$	Electromechanical
$\lambda_{3\&4}$	$-1.5704 \pm j11.4504$	1.8224	0.1359	$\boldsymbol{\omega_{r_8}}$,$\boldsymbol{\delta_{GFM_3}}$,$\boldsymbol{\delta_{r_8}}$,$\omega_{GFM_3}$,E'_{q_8}	Electromechanical
$\lambda_{5\&6}$	$-0.7167 \pm j11.2226$	1.7861	0.0637	$\boldsymbol{\delta_{GFM_1}}$,$\boldsymbol{\omega_{GFM_1}}$,$\omega_{GFM3}$	Electromechanical
$\lambda_{7\&8}$	$-1.6783 \pm j10.6958$	1.7023	0.1550	$\boldsymbol{\omega_{r_8}}$,$\boldsymbol{\delta_{r_8}}$,$E'_{q_8}$,$\omega_{r_4}$,$\delta_{GFM_3}$,$\omega_{r_{GFM3}}$, ω_{r_9}	Electromechanical
$\lambda_{9\&10}$	$-1.0650 \pm j7.4529$	1.1862	0.1415	$\boldsymbol{\delta_{r_9}}$,$\boldsymbol{\omega_{r_9}}$,$\delta_{GFM_3}$,$\omega_{r_{10}}$,E'_{q_9}	Electromechanical

Subscript numbers refer to the machine number which can be seen in Fig. 1.

TABLE III. EIGENVALUES OF INTEREST FOR MULTI-LOOP CONTROL SCENARIO

Eigenvalue	Coordinates	Frequency (Hz)	Damping Ratio	Dominant States	Category
$\lambda_{11\&12}$	$-0.5577 \pm j12.4033$	1.9740	0.0449	$\boldsymbol{\omega_{GFM_2}}$,$\boldsymbol{\delta_{GFM_2}}$,$\omega_{r_4}$,$\delta_{GFM_3}$,$\delta_{GFM_1}$	Electromechanical
$\lambda_{13\&14}$	$-1.5240 \pm j11.8298$	1.8828	0.1278	$\boldsymbol{\omega_{r_8}}$,$\boldsymbol{\delta_{GFM_3}}$,$\omega_{GFM_3}$,$\delta_{r_8}$,$E'_{q_8}$	Electromechanical
$\lambda_{15\&16}$	$-0.7015 \pm j11.4685$	1.8253	0.0610	$\boldsymbol{\delta_{GFM_1}}$,$\boldsymbol{\omega_{GFM_1}}$,$\omega_{GFM_3}$	Electromechanical
$\lambda_{17\&18}$	$-1.7469 \pm j10.6211$	1.6904	0.1623	$\boldsymbol{\omega_{r_8}}$,$\boldsymbol{\delta_{r_8}}$,$E'_{q_8}$,$\omega_{r_4}$,$\omega_{r_9}$,$\delta_{GFM_3}$	Electromechanical
$\lambda_{19\&20}$	$-0.9950 \pm j7.4804$	1.1905	0.1319	$\boldsymbol{\delta_{r_9}}$,$\boldsymbol{\omega_{r_9}}$,$\omega_{r_{10}}$,$\delta_{GFM_3}$,$E'_{q_9}$	Electromechanical
$\lambda_{21\&22}$	$-0.6295 \pm j7.0821$	1.1272	0.0885	$\boldsymbol{\delta_{r_{10}}}$,$\boldsymbol{\omega_{r_{10}}}$,$\omega_{r_2}$,$\delta_{GFM_3}$	Electromechanical
$\lambda_{23\&24}$	$-0.2350 \pm j0.0770$	0.0123	0.9503	$\boldsymbol{\gamma_{CC2_2}}$, $\boldsymbol{\gamma_{CC1_2}}$,$\boldsymbol{\omega_{r_1}}$	Inner *CC*-related
$\lambda_{25\&26}$	$-0.0526 \pm j0.0541$	0.0086	0.6970	$\boldsymbol{\gamma_{CC1_2}}$,$\gamma_{PSS_{3_7}}$, γ_{CC2_2},$\gamma_{PSS_{3_6}}$, γ_{CC1_1}, γ_{CC1_3},ω_{r_1}	Inner *CC*-related
λ_{27}	-0.2373	0	1	$\boldsymbol{\gamma_{CC2_1}}$, $\boldsymbol{\gamma_{CC1_1}}$, γ_{CC2_2}	Inner *CC*-related
λ_{28}	-0.2131	0	1	$\boldsymbol{\gamma_{CC2_3}}$, $\boldsymbol{\gamma_{CC2_2}}$, γ_{CC1_3}, γ_{CC2_1}	Inner *CC*-related
λ_{29}	-0.0670	0	1	$\boldsymbol{\gamma_{CC1_1}}$,$\boldsymbol{\gamma_{CC1_2}}$,$\boldsymbol{\gamma_{CC2_1}}$, γ_{CC2_2}	Inner *CC*-related
λ_{30}	-0.0847	0	1	$\boldsymbol{\gamma_{CC1_3}}$,$\boldsymbol{\gamma_{CC1_1}}$,$\gamma_{PSS_{3_9}}$,$\gamma_{CC1_2}$,$\gamma_{CC2_3}$,$\gamma_{PSS_{3_7}}$	Inner *CC*-related
$\lambda_{31\&32}$	$-0.00000352 \pm j0.000797$	0.000012689	0.0044	$\boldsymbol{\gamma_{VC2_1}}$,$\boldsymbol{\gamma_{VC1_1}}$, $\boldsymbol{\gamma_{VC2_2}}$, $\boldsymbol{\gamma_{VC1_2}}$, $\boldsymbol{\gamma_{VC2_3}}$, $\boldsymbol{\gamma_{VC1_3}}$	Inner *VC*-related
$\lambda_{33\&34}$	$-0.00000773 \pm j0.000801$	0.000012747	0.0097	$\boldsymbol{\gamma_{VC1_3}}$,$\boldsymbol{\gamma_{VC2_3}}$,$\boldsymbol{\gamma_{VC1_1}}$,$\boldsymbol{\gamma_{VC2_1}}$	Inner *VC*-related
$\lambda_{35\&36}$	$-0.00000930 \pm j0.000803$	0.000012783	0.0116	$\boldsymbol{\gamma_{VC1_2}}$,$\boldsymbol{\gamma_{VC2_2}}$,$\boldsymbol{\gamma_{VC1_1}}$,$\boldsymbol{\gamma_{VC2_1}}$	Inner *VC*-related

of these modes is also confirmed with the participation factors showing dominant modes associated with the rotor speed and angle of SGs with ω_r and δ_r, as well as the GFMs with ω_{GFM} and δ_{GFM}. There is also some small participation from states associated with the rotor field windings, $E_q^{'}$. All modes involve multiple generators (GFMs and/or SGs). Additionally, for this timescale, all modes are well damped, with the minimum being 4.81 %. Typically, a damping ratio of above 3 % is considered sufficient for EMc modes.

IV. GFMS WITH MULTI-LOOP CONTROL

The eigenvalues and their characteristics for this set up are displayed in Table III. We find the same EMc modes as observed in Table II with small changes to the frequency and damping. However, there are additional modes now found to be of interest. All of the additional modes are in close proximity to the stability boundary and are related to the inner controllers of the GFMs. The inner CC states are denoted by $\gamma_{CC_{1\&2}}$ and the inner VC states are denoted by $\gamma_{VC_{1\&2}}$. The eigenvalues can be split into three main categories: EMc, inner CC-related, and inner VC-related. The inner CC-related modes, λ_{23to30}, are seen to be low frequency or non-oscillatory and may have participation from the PSSs of SGs, whose states are denoted by $\gamma_{PSS_{1\&2\&3}}$, or even the rotor speed dynamics as in $\lambda_{23\&24}$ and $\lambda_{25\&26}$. The inner VC-related modes, λ_{31to36} are seen to be very close to the origin with very low frequency and close to the unstable region. It is important to note that all of the inner controller related modes except $\lambda_{23\&24}$ involve the inner controllers of multiple (or all) GFMs throughout the system, proving the need to perform system-level small signal studies.

An additional note of interest is the lack of any important modes consisting of interactions between the GFM control states and the network dynamics. Likely due to the restricted control bandwidth of the GFMs, this might suggest the possibility of model order reduction in relation to time separation for an algebraic representation of the network.

V. PARAMETRIC SENSITIVITY ANALYSIS

Parametric sweeps are performed for the multi-loop case and are displayed in Fig. 3 to further the understanding of how the identified mode categories can be influenced. Note, the sweeps of any given parameter are performed on all the GFMs at once. From Fig. 3a we can observe that the damping factor, ζ, associated with the tuning of the inner VC has a small impact on the inner CC-related modes and significant influence over the stability of the inner VC-related interactions. For the latter, the real-parts curve from instability into the stable region and then back towards the instability boundary but without reaching

it. The chosen parameter value for the base case investigated previously was 25, at approximately the maximum negative real part for these modes within the range investigated. Fig. 3b displays the influence that the inner CC time constant, τ_{CC}, (and hence inner VC time constant) has over the inner controller related modes. When considering the inner VC-related modes specifically, the increase of τ_{CC} brings the eigenvalues closer to the origin.

Moving our attention to the slower outer controllers, Fig. 3c confirms that the inertia constant, H_{apc}, has a significant impact on the EMc modes with the potential for instability to occur if the parameter is set too high. H_{apc} can also be seen to have an impact on the inner CC-related modes but to a lesser extent and causing no instability in this case. In terms of the VC-related interactions, H_{apc} has no impact. The damping constant, D_{apc}, is also seen to have significant impact on the EMc modes in Fig. 3d. However, for the range of parameter values evaluated no instability is observed. Similar to H_{apc}, D_{apc} has a small impact on the inner CC-related modes, without causing any issues in this case, and has no impact at all on the inner VC-related modes. The final parametric sweep in Fig. 3e finds that the reactive power droop gain, m_q, has negligible impact on the EMc modes as well as the inner CC-related modes. However, it does impact the inner VC-related interactions with increasing values bringing increased damping.

It should be noted that the conclusions drawn from these results are specific to the test system utilised at the operating point of interest. Also, the elements connected to the system and their specific parameter tuning values will have significant impact on the small signal behaviour. This work aims to shed light on potential interactions that can occur in transmission systems containing a mix of SGs and GFMs.

VI. Conclusions

This paper provides a small signal analysis focusing on multi-machine interactions in a GFM-penetrated transmission network. More specifically, this work utilises a modified IEEE 39-bus system with the addition of CIG utilising the VSM GFM control scheme (with and without inner loops). The interactions observed are split into three main categories of EMc, inner-VC related, and inner-CC related modes. The latter of which might also involve the PSSs, or even the rotor speed dynamics, of SGs. It was found that all types of mode typically involve participation from multiple machines (GFMs and/or SGs) within the system.

The sensitivity of these interactions to different GFM parameters is also investigated for this specific system. The inner VC tuning damping factor is important for stabilising the inner VC-related multi-unit interactions. The inner controller time constant has influence over the inner CC-related modes. There is a destabilising impact on EMc modes from the virtual inertia constant of the VSM. The virtual damping constant and reactive power droop gain have less impact on the overall stability of the system. Although, they do have some influence over the EMc and inner-VC related modes, respectively. For this test system, it can be determined that removing the inner VCs would be beneficial. Maintaining the inner CCs would be sufficient for the current reference limitation approach and although inner CC-related modes are close to the stability boundary, they cause no stability issues (in this case).

References

[1] C. N. Hatziargyriou *et al.*, "Definition and Classification of Power System Stability – Revisited & Extended," *IEEE Trans. Power Syst.*, vol. 6, no. 4, pp. 3271–3281, 2021.

[2] N. Pogaku, M. Prodanović, and T. C. Green, "Modeling, analysis and testing of autonomous operation of an inverter-based microgrid," *IEEE Trans. Power Electron.*, vol. 22, no. 2, pp. 613–625, Mar. 2007, doi: 10.1109/TPEL.2006.890003.

[3] W. Du *et al.*, "A Comparative Study of Two Widely Used Grid-Forming Droop Controls on Microgrid Small-Signal Stability," *IEEE J. Emerg. Sel. Top. Power Electron.*, vol. 8, no. 2, pp. 963–975, 2020.

[4] M. Ndreko, S. Rüberg, and W. Winter, "Grid forming control scheme for power systems with up to 100% power electronic interfaced generation: A case study on Great Britain test system," *IET Renew. Power Gener.*, vol. 14, no. 8, pp. 1268–1281, 2020.

[5] U. Markovic *et al.*, "Understanding Small-Signal Stability of Low-Inertia Systems," *IEEE Trans. Power Syst.*, vol. 36, no. 5, pp. 3997–4017, 2021.

[6] Y. Liao, X. Wang, F. Liu, K. Xin, and Y. Liu, "Sub-Synchronous Control Interaction in Grid-Forming VSCs with Droop Control," in *2019 4th IEEE Workshop on the Electronic Grid*, 2019, pp. 1–6.

[7] S. Leitner, M. Yazdanian, A. Mehrizi-Sani, and A. Muetze, "Small-Signal Stability Analysis of an Inverter-Based Microgrid with Internal Model-Based Controllers," *IEEE Trans. Smart Grid*, vol. 9, no. 5, pp. 5393–5402, Sep. 2018, doi: 10.1109/TSG.2017.2688481.

[8] S. Dong and Y. C. Chen, "Analysis of Feasible Synchronverter Pole-placement Region to Facilitate Parameter Tuning," *IEEE Trans. Energ*, 2021, doi: 10.1109/TEC.2021.3068758.

[9] T. Qoria, C. Li, K. Oue, F. Gruson, F. Colas, and X. Guillaud, "Direct AC voltage control for grid-forming inverters," *J. Power Electron.*, vol. 20, no. 1, pp. 198–211, 2020.

[10] R. Rosso, S. Engelken, and M. Liserre, "Current Limitation Strategy For Grid-Forming Converters Under Symmetrical And Asymmetrical Grid Faults," in *2020 IEEE Energy Conversion Congress and Exposition*, 2020, vol. 1, pp. 3746–3753.

[11] X. Wang, Y. W. Li, S. Member, and F. Blaabjerg, "Virtual-Impedance-Based Control for Voltage-Source and Current-Source Converters," *IEEE Trans. Power Electron.*, vol. 30, no. 12, pp. 7019–7037, 2015, doi: 10.1109/TPEL.2014.2382565.

[12] S. D. Arco, J. A. Suul, O. B. Fosso, and S. Member, "Automatic Tuning of Cascaded Controllers for Power Converters Using Eigenvalue Parametric Sensitivities," *IEEE Trans. Ind. Appl.*, vol. 51, no. 2, pp. 1743–1753, 2015, doi: 10.1109/TIA.2014.2354732.

[13] T. Qoria, F. Gruson, F. Colas, and X. Guillaud, "Tuning of cascaded controllers for robust grid-forming Voltage Source Converter," in *2018 Power Systems Computation Conference (PSCC)*, 2018.

[14] S. D'Arco and J. A. Suul, "Equivalence of Virtual Synchronous Machines and Frequency-Droops for Converter-Based MicroGrids," *IEEE Trans. Smart Grid*, vol. 5, no. 1, pp. 394–395, 2014.

[15] P. S. Kundur, *Power System Stability and Control*, Third. New York: McGraw-Hill, 2017.

[16] R. D. Zimmerman and C. E. Murillo-Sánchez, "Matpower: User's Manual," 2020. [Online]. Available: https://matpower.org/doc/.

[17] P. Peter W., Sauer; M. A., *Power System Dynamics and Stability*. Urbana: The University of Illinois, 1997.

[18] IEEE PES Task Force on Benchmark Systems for Stability Controls, "Report on the EMTP-RV 39-bus system (New England Reduced Model)," 2015. [Online]. Available: http://www.sel.eesc.usp.br/ieee/.

[19] A. Egea-Alvarez, A. Junyent-Ferré, and O. Gomis-Bellmunt, "Active and Reactive Power Control of Grid Connected Distributed Generation Systems," in *Modeling and Control of Sustainable Power Systems*, 2012, pp. 47–81.